Giant enhancement of optical high-order sideband generation and their control in a dimer of two cavities with gain and loss

Jiahui Li,[1,*] Jiahua Li,[1,2,†] Qian Xiao,[1] and Ying Wu[1,‡]

[1]*School of Physics and Wuhan National Laboratory for Optoelectronics, Huazhong University of Science and Technology, Wuhan 430074, People's Republic of China*

[2]*MOE Key Laboratory of Fundamental Physical Quantities Measurement, Huazhong University of Science and Technology, Wuhan 430074, People's Republic of China*

(Received 12 April 2016; published 9 June 2016)

Parity-time ($\mathcal{PT}$) symmetric systems, which rely on the balanced gain-loss condition and render the Hamiltonian non-Hermitian, have provided a new platform to engineer effective light-matter interactions in recent years. Here we explore the high-order sideband features of the output fields obtained from a $\mathcal{PT}$-symmetric optical system consisting of a passive nonlinear cavity coupled to an active linear cavity. By employing a perturbation technique, we derive analytic formulas used to determine the nonlinear transmission coefficient of optical second-order sideband in this structure. Using experimentally achievable parameters, it is clearly shown that the efficiency of the second-order sideband generation can be greatly enhanced in the $\mathcal{PT}$-symmetric dimer, extremely in the vicinity of the transition point from unbroken- to broken-$\mathcal{PT}$ regimes. Moreover, we further analyzed the influences of the system parameters, including the photon-tunneling rate between two cavities, Kerr nonlinearity strength, and optical detuning, on the second-order sideband generation. Subsequently we investigate the higher-order sideband output spectrum by numerical simulations, where the sideband amplitude also is largely enhanced in the $\mathcal{PT}$-symmetric arrangement, compared with the passive-passive double-cavity system. Our obtained results provide a new avenue for acquiring optical high-order sidebands and operating light, which may inspire further applications in chip-scale optical communications and optical frequency combs.

DOI: 10.1103/PhysRevA.93.063814

I. INTRODUCTION

As one of mainly branches of optics science, nonlinear optics describes the light features in the nonlinear media, giving rise to abundant novel optical phenomena [1]. From laser technology to optical spectroscopy to quantum optics, the nonlinear interactions have been at the forefront of many research disciplines. As one of prominent nonlinear effects, optical high-order harmonic generation was first discovered by Franken [2] and has developed potential applications in optical communication and atto-physics. Similar to optical high-order harmonic generation in atoms or molecules, optical high-order sideband generation is also a process of new frequencies generation when a photonic system (e.g., photonic crystal molecule or cavity optomechanical system) is illuminated by lasers with different frequencies [3–6]. However, these nonlinear optical effects only can be observed at very high light intensities for the weak nonlinearity in bulk materials, which poses a serious hurdle to implement relative applications in digital optical computing.

Bender and Boettcher showed that some non-Hermitian Hamiltonians can exhibit real eigenvalue spectra as long as they preserve the parity-time ($\mathcal{PT}$) symmetry [7–9]. Since then, considerable researches have been motivated in a variety of physical systems due to the great potential of $\mathcal{PT}$-symmetric system in both fundamental physics and practical applications [10–20]. The particularity of a $\mathcal{PT}$-symmetric system lies in that the system processes a phase transition (spontaneous $\mathcal{PT}$-symmetry breaking) as the system parameters are properly tuned. The spontaneous $\mathcal{PT}$-symmetry breaking point is also called an exceptional point (EP), which can significantly influence the dynamics of system and distinguish the $\mathcal{PT}$-symmetric phase and $\mathcal{PT}$-broken phase. When the parameter controlling the degree of the non-Hermiticity exceeds the so-called EP, the system Hamiltonian has completely real eigenvalues and shares uniform eigenfunctions with the $\mathcal{PT}$ operator. Otherwise, the eigenvalues become complex, and the eigenfunctions of the Hamiltonian and $\mathcal{PT}$ operator are different from each other. As the most productive and versatile platform to explore $\mathcal{PT}$-symmetric applications, an optical $\mathcal{PT}$-symmetric system was theoretically proposed and experimentally demonstrated by coupled optical wave guides [21,22], transmission lines, whispering-gallery-mode resonators [23–25], cavity optomechanical systems [26], and optical lattices [27–31]. Remarkable advances have been made in those optical components, such as nonreciprocal light transmission [32–35], low-power optical diodes [36–38] or sensors [39,40], efficient photon and phonon lasing [41–45] or laser absorbers [46,47], loss-induced or gain-induced transparency [48,49], optical parametric amplification via non-Hermitian phase matching [50], and $\mathcal{PT}$-broken chaos [51], just to name a few examples. Naturally this raises a question whether greatly enhanced high-order sideband generation can appear in such an optical $\mathcal{PT}$-symmetric system. Clearly seeking an easy and robust way to control the high-order sidebands is an undoubted challenge from both scientific and technological viewpoints.

In order to answer and address the above-mentioned issue, in the present work we systematically explore the nonlinear

*lijiahui928@163.com

†Author to whom correspondence should be addressed: huajia_li@163.com; http://qoap.phys.hust.edu.cn/

‡yingwu2@126.com

transmission characteristics of optical high-order sidebands in an optical $\mathcal{PT}$-symmetric system. The system employed is composed of two directly coupled microcavities, coherently driven by a bichromatic laser field. Gain in one of the two cavities is provided by optically pumping the doped erbium ions; the other one without dopant exhibits passive loss [38]. Moreover, the weak nonlinearity is assumed to exist only in the passive cavity. By taking advantage of the perturbation approach, we present an explicit method to calculate the nonlinear transmission coefficient of an optical second-order sideband. The efficiency of the second-order sideband generation shows a giant amplitude enhancement of about six orders of magnitude with respect to the passive-passive double-cavity system. Also, we explore the higher-order sideband output spectrum by numerical simulations. It is found that the higher-order sideband amplitude is largely enhanced in the $\mathcal{PT}$-symmetric arrangement as well. The physical mechanism underlying this is rooted in the localization-induced dynamical intensity accumulation in the $\mathcal{PT}$-symmetric system. Comparing with the passive-passive double-cavity system, strong effective optical nonlinearity can be achieved in the $\mathcal{PT}$-symmetric optical system at a very low input level [52,53]. Consequently, the amplified second-order sideband as well as optical higher-order sideband signals can be achieved efficiently in the $\mathcal{PT}$-symmetric architecture.

We note that the nonlinearity improved by an optical $\mathcal{PT}$-symmetric system also has been studied in Ref. [54], where a passive microcavity containing a single quantum emitter (QE) couples with an active microcavity. The linear transmission rate and the optical third-order nonlinearities derived from the QE-cavity coupling were enhanced efficiently in the system when the phase transition occurs. Nevertheless, in the present proposed $\mathcal{PT}$-symmetric system (see Fig. 1), greatly enhanced optical high-order sideband generation and their easy and robust control by properly adjusting the system parameters have remained elusive for this pursuit so far. Compared to Ref. [54], the driving approach of the system and the method of the optical nonlinearity produced are quite different. Here

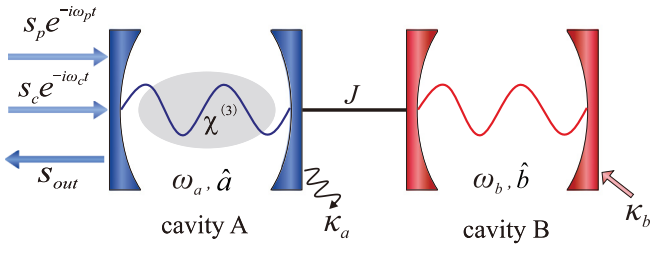

FIG. 1. Schematic illustration of a $\mathcal{PT}$-symmetric device including a passive cavity coupled to an active cavity with coupling strength J (also called photon-tunneling rate). The passive cavity A has a weak nonlinearity where a Kerr nonlinear optical medium is embedded and is driven with a bichromatic field at a rate of κ_e. Here κ_a denotes the total loss rate of the cavity A, which contains an intrinsic loss rate and an external loss rate. κ_b denotes the effective loss rate of the cavity B, which is reduced by external gain g with the relationship $\kappa_b = \kappa_b^i - g$ (κ_b^i is the intrinsic loss rate of the cavity B). We suppose that $\kappa_b > 0$ corresponds to a passive loss cavity, and $\kappa_b < 0$ corresponds to an active gain one.

we use a device of optical coupled microcavities with weak Kerr-type nanostructure materials, where the nonlinearity comes from the interactions between the light and three-order nonlinear materials, and the device is coherently driven by a bichromatic (i.e., two-tone) laser. However, in Ref. [54] the nonlinearity derived from photon-photon interactions via a single quantum emitter coupled to a monochromatic driven cavity. As is well known, both multichromatic driving and optical nonlinearity are necessary conditions for generating optical high-order sideband. Namely, the device in Ref. [54] cannot generate the optical high-order sidebands by means of such a monochromatic driving laser.

This paper is structured as follows: In Sec. II we present the physical model of a nonlinear $\mathcal{PT}$-symmetric cavity dimer. Making use of the perturbation technique, we give the detailed derivation of analytical expression for the transmission coefficient of the second-order sideband and describe the physical quantities of interest. In Sec. III, by comparing with the passive-passive double-cavity system, we study the enhancement of the second-order and higher-order sideband generation in the $\mathcal{PT}$-symmetric system. We also discuss the influences of the coupling strength between two cavities, Kerr nonlinearity strength, and optical detuning on the second-order sideband generation in this section. In Sec. IV we give the feasibility of implementing our theoretical method in this $\mathcal{PT}$-symmetric system. Finally, we conclude our results in Sec. V.

II. PROPOSED MODEL AND BASIC FORMULA

As schematically shown in Fig. 1, the system is composed of two coupled single-mode cavities, one of which has cavity loss and weak nonlinearity, and the other has cavity gain but no nonlinearity. Owing to the finite overlap of the cavity modes, two cavities can directly couple by the coherent photon tunneling with strength J, which can be efficiently modulated by the distance between them. We assume that the cavity A is simultaneously driven by a strong control field of frequency ω_c and a weak probe field of frequency ω_p, denoted by $S_{\rm in} = s_c e^{-i\omega_c t} + s_p e^{-i\omega_p t}$. s_c and s_p are the amplitudes of the control field and the probe field, which are directly related to the control-field power $P_c = \hbar\omega_c s_c^2$ and the probe-field power $P_p = \hbar\omega_p s_p^2$.

The Hamiltonian describing this composite system is yielded in a rotating frame at the frequency of the control laser ω_c by

$$\mathcal{H} = \hbar\Delta(\hat{a}^\dagger\hat{a} + \hat{b}^\dagger\hat{b}) + U\hat{a}^\dagger\hat{a}^\dagger\hat{a}\hat{a} + \hbar J(\hat{a}^\dagger\hat{b} + \hat{a}\hat{b}^\dagger) + i\hbar\sqrt{\kappa_e}[(s_c + s_p e^{-i\Omega t})\hat{a}^\dagger - \text{H.c.}], \quad (1)$$

where $\hat{a}$ ($\hat{b}$) and $\hat{a}^\dagger(\hat{b}^\dagger)$ are the annihilation and creation operators of the cavity A (B) with resonance frequency ω_a (ω_b), respectively, with the commutation relations $[\hat{a},\hat{a}^\dagger] = 1$ and $[\hat{b},\hat{b}^\dagger] = 1$. For the $\mathcal{PT}$-symmetric structure, above we have assumed that the resonance frequencies of both cavities are equal, i.e., $\omega_a = \omega_b = \omega$. U is the Kerr nonlinear interaction strength. κ_e denotes the external loss rate of the passive cavity A, derived from the interaction between the cavity A and the external field, related to the coupling quality factor Q_e by $\kappa_e = \omega_a/Q_e$ (see Fig. 1). The frequency detunings

between the cavity field, the control laser, and the probe laser are represented by $\Delta = \omega - \omega_c$, $\Delta_p = \omega_p - \omega$, and $\Omega = \omega_p - \omega_c = \Delta_p + \Delta$, respectively.

In our work, we apply the semiclassical Heisenberg-Langevin equations to describe the evolution of this $\mathcal{PT}$-symmetric system and consider the expectation values of all the operators. Taking the cavity damping and the cavity excitation processes into consideration, we can get the equations of motion for the $\mathcal{PT}$-symmetric system as follows:

$$\frac{da}{dt} = -\left(i\Delta + \frac{\kappa_a}{2}\right)a - 2iU|a|^2 a - iJb + \sqrt{\kappa_e}(s_c + s_p e^{-i\Omega t}), \tag{2}$$

$$\frac{db}{dt} = -\left(i\Delta + \frac{\kappa_b}{2}\right)b - iJa, \tag{3}$$

where κ_a and κ_b are total loss rates of the cavity A and B, respectively. Note that, $\kappa_a > 0$, $\kappa_b > 0$ in the Eqs. (2) and (3) correspond to a passive-passive double-cavity system, and yet $\kappa_a > 0$, $\kappa_b < 0$ correspond to a passive-active double-cavity system.

It be should pointed out that, the above nonlinear equations (2) and (3) cannot be solved exactly, because the steady-state response contains an infinite number of components of different frequencies. As the control field is much stronger than the probe filed, we can use the perturbation method [55] to deal with Eqs. (2) and (3). To this end, the total solution of the intracavity field can be written as $a = a_s + \delta a$, $b = b_s + \delta b$, where a_s, b_s are the steady-state solutions when $s_p = 0$. By using the above ansatz, we obtain the following steady-state solutions

$$a_s = \frac{\sqrt{\kappa_e} s_c}{\Delta_a + \frac{J^2}{\Delta_b} + 2iU|a_s|^2}, \tag{4}$$

$$b_s = \frac{-iJa_s}{\Delta_b}, \tag{5}$$

where we have defined $\Delta_a = i\Delta + \kappa_a/2$ and $\Delta_b = i\Delta + \kappa_b/2$, respectively.

We assume that the perturbation terms δ_a and δ_b have the following forms [55]:

$$\delta a = A_1^- e^{-i\Omega t} + A_1^+ e^{i\Omega t} + A_2^- e^{-2i\Omega t} + A_2^+ e^{2i\Omega t} + \cdots, \tag{6}$$

$$\delta b = B_1^- e^{-i\Omega t} + B_1^+ e^{i\Omega t} + B_2^- e^{-2i\Omega t} + B_2^+ e^{2i\Omega t} + \cdots. \tag{7}$$

The physical picture of such an ansatz (6) or (7) is that when the control field and the probe field are incident upon the cavity A, there are the output fields generated with a series of frequencies $\omega_c \pm n\Omega$, due to the nonlinear interaction of this system, where n is an integer representing the order of the sideband. The first upper sideband is referred to as the anti-Stokes field, and the first lower sideband is know as the Stokes field. The output field with a frequency $\omega_c + 2\Omega$ is the second-order upper sideband, while the frequency $\omega_c - 2\Omega$ is the second-order lower sideband. We consider only the first and second-order sidebands; the higher-order sidebands are ignored here because they can be obtained in a similar fashion. The signals at the second- and high-order sidebands are of great importance in understanding the nonlinear interactions. Here the parameters A_1^- and A_1^+ are the coefficients of first upper and lower sidebands, and much smaller than a_s. Similarly, A_2^- and A_2^+ are the coefficients of the second upper and lower sidebands and much smaller than A_1^- and A_1^+. These parameters can be obtained by substituting Eqs. (6)–(7) into Eqs. (2)–(3) and comparing the coefficients of the same order. After some calculations, we can get the result

$$A_1^- = \frac{(F_1^+)^*}{F_1^-(F_1^+)^* - 4U^2|a_s|^4}\sqrt{\kappa_e} s_p, \tag{8}$$

and A_1^+ can be expressed with A_1^- as

$$A_1^+ = \frac{-2iUa_s^2}{F_1^+}(A_1^-)^*, \tag{9}$$

with

$$F_1^- = -i\Omega + \frac{J^2}{-i\Omega + \Delta_b} + \Delta_a + 4iU|a_s|^2, \tag{10}$$

$$F_1^+ = i\Omega + \frac{J^2}{i\Omega + \Delta_b} + \Delta_a + 4iU|a_s|^2. \tag{11}$$

The amplitude of the second-order optical sideband A_2^-, the quantity of interest here, can be obtained as (in terms of A_1^-)

$$A_2^- = \frac{M + N}{[F_2^-(F_2^+)^* - 4U^2|a_s|^4][(F_1^+)^*]^2}(A_1^-)^2, \tag{12}$$

and A_2^+ can be expressed with A_1^-, A_1^+, and A_2^- as

$$A_2^+ = -\frac{2iU[2a_s A_1^+(A_1^-)^* + a_s^*(A_1^+)^2]}{F_2^+} - \frac{2iUa_s^2}{F_2^+}(A_2^-)^*, \tag{13}$$

where the parameters F_2^- and F_2^+ are defined by

$$F_2^- = -2i\Omega + \frac{J^2}{-2i\Omega + \Delta_b} + \Delta_a + 4iU|a_s|^2, \tag{14}$$

$$F_2^+ = 2i\Omega + \frac{J^2}{2i\Omega + \Delta_b} + \Delta_a + 4iU|a_s|^2, \tag{15}$$

and from Eqs. (14)–(15) the parameters M and N are given by

$$M = -16U^4|a_s|^6 a_s^* + 8U^2|a_s|^2 a_s^*(F_1^+)^*(F_2^+)^*, \tag{16}$$

$$N = 16iU^3|a_s|^4 a_s^*(F_1^+)^* - 2iUa_s^*(F_2^+)^*[(F_1^+)^*]^2. \tag{17}$$

By applying the input-output relation $S_{\text{out}} = S_{\text{in}} - \sqrt{\kappa_e}a$, the output field can be written as

$$S_{\text{out}} = c_0 + c_1^- e^{-i\Omega t} + c_1^+ e^{i\Omega t} + c_2^- e^{-2i\Omega t} + c_2^+ e^{2i\Omega t}, \tag{18}$$

with the coefficients $c_0 = s_c - \sqrt{\kappa_e}a_s$, $c_1^- = s_p - \sqrt{\kappa_e}A_1^-$, $c_1^+ = -\sqrt{\kappa_e}A_1^+$, $c_2^- = -\sqrt{\kappa_e}A_2^-$, and $c_2^+ = -\sqrt{\kappa_e}A_2^+$, respectively. It should be emphasized that these results have a shift of a frequency ω_c, because the Heisenberg-Langevin equations describe the evolution of the optical field in a rotating frame at the frequency ω_c. c_0 is one of components corresponding to the control field with frequency ω_c. And c_1^- responding to

the probe field with frequency ω_p, is the coefficient of the first upper sideband (anti-Stokes field). The transmission of the probe field is defined as $t_p = c_1^-/s_p$. Since A_1^- has been given by Eq. (8), the optical transmission rate can be expressed as

$$|t_p|^2 = \left|1 - \frac{\kappa_e (F_1^+)^*}{F_1^-(F_1^+)^* - 4U^2|a_s|^4}\right|^2. \tag{19}$$

Finally, the term c_2^- describes the second-order upper sideband process, in which the output field with frequency $\omega_c + 2\Omega$ can be produced. The term c_2^+ describes the second-order lower sideband process, in which the output field with frequency $\omega_c - 2\Omega$ is produced. In order to discuss the effect induced by the second-order sideband in this $\mathcal{PT}$-symmetric system, we introduce the dimensionless quantity

$$\eta = |-\sqrt{\kappa_e} A_2^-/s_p| \tag{20}$$

and

$$\beta = |-\sqrt{\kappa_e} A_2^+/s_p| \tag{21}$$

to describe the efficiency of the optical second-order sideband process. In the following, we will discuss in detail the generation of the second-order upper sideband, where Eq. (20) is the central result of this paper. One also can investigate the generation of the second-order lower sideband by using Eq. (21) with the same method, while the results of β are not shown here due to similar characteristics and the space limitation.

III. ENHANCEMENT OF THE HIGH-ORDER SIDEBAND GENERATION IN THE $\mathcal{PT}$-SYMMETRIC SYSTEM

In this section, we first focus on the properties of the second-order sideband for two possible configurations (passive-passive double cavity and $\mathcal{PT}$-symmetric cavity arrangement) based on the analytical expression (20). In this situation, we in details analyze the influences of the system parameters, including the photon-tunneling rate between two cavities, Kerr nonlinearity strength, and optical detuning, on the second-order sideband generation. Note that an ultralow control-field power is used in our proposal, choosing $P_c = 0.1\mu$W. At the same time, the amplitude of the probe field is hundred times less than the amplitude of the control field, e.g., $s_p/s_c = 0.01$. Next, we turn to illustrate the higher-order sideband output spectrum by numerical simulations directly based on Eqs. (2) and (3).

A. Dependence of the second-order sideband on the photon-tunneling rate J

First, we start by evaluating the efficiency of the second-order sideband generation η as a function of the probe detuning Δ_p ($\Delta_p = \omega_p - \omega$) for a passive-passive double-cavity system (i.e., non-$\mathcal{PT}$-symmetric system) by plotting Figs. 2(a) and 2(b). For a small value of the coupling strength J, the spectrum of η shows two symmetric sideband peaks and a shallow resonance dip as shown in Fig. 2(a). With the increase of J, the peaks shift towards both sides, and the dip becomes

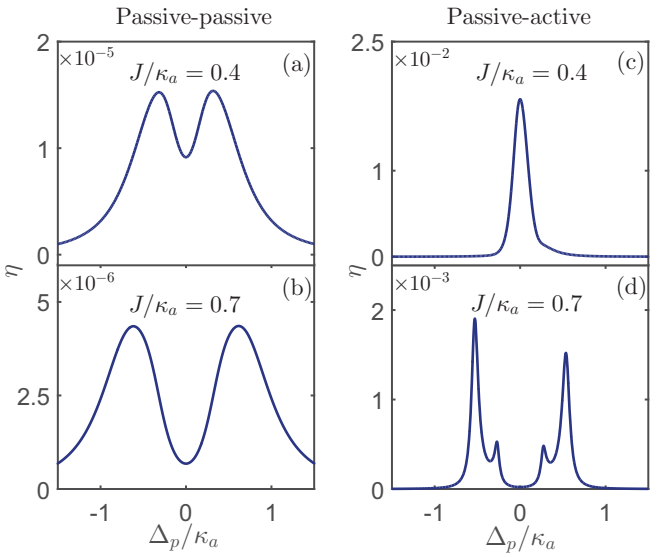

FIG. 2. Calculation result of η as a function of the detuning Δ_p/κ_a under two different values of the coupling strength J for the passive-passive double-cavity system (i.e., $\kappa_b/\kappa_a = 0.8$) in panels (a) and (b) and the passive-active double-cavity $\mathcal{PT}$ system (i.e., $\kappa_b/\kappa_a = -0.8$) in panels (c) and (d). According to recent microcavity experiments [36,38], we use the coupling strength $J/\kappa_a = 0.4$ in panels (a) and (c) and $J/\kappa_a = 0.7$ in panels (b) and (d). The other system parameters are $\omega_c/2\pi = 200$ THz, $\kappa_a/2\pi = 100$ MHz, $\kappa_e/\kappa_a = 0.5$, $\Delta = 0$, and $U/\kappa_a = 10^{-6}$, respectively.

wider. Alternatively, the value of η is reduced rapidly, denoting that the generation of the second-order sideband tends to be suppressed by the strong photon-tunneling effect in the passive-passive double-cavity system as shown in Fig. 2(b). Then we focus on the second-order sideband generation in a passive-active double-cavity system (i.e., $\mathcal{PT}$-symmetric system) with a fixed gain-to-loss ratio $\kappa_b/\kappa_a = -0.8$. By changing the coupling strength J between two cavities, we can tune the optical system transiting from the $\mathcal{PT}$-broken phase to the $\mathcal{PT}$-symmetric phase. When $J/\kappa_a < 0.45$, the system is in the $\mathcal{PT}$-broken phase. It can be seen from Fig. 2(c) that the second-order sideband features a single sideband peak, which reaches its maximum at $\Delta_p = 0$. As J increases from $0.4\kappa_a$ to $0.7\kappa_a$ in Fig. 2(d), the system enters into the $\mathcal{PT}$-symmetric phase for $J/\kappa_a > 0.45$. The spectrum of η displays two sideband peaks, each of which has a small peak nearby. Particularly, the sideband peak on the left side is slight higher than the right one. Moveover, in sharp contrast to Figs. 2(a) and 2(b), the values of η in Figs. 2(c) and 2(d) are greatly improved for about three orders of magnitude. This implies that $\mathcal{PT}$-symmetric structure can amplify the second-order sideband signal effectively.

The logarithm of the maximum value of η varying with the coupling strength J is plotted in Fig. 3(a) corresponding to a passive-passive double-cavity system and Fig. 3(b) corresponding to a passive-active double-cavity $\mathcal{PT}$ system. In the limit of $J/\kappa_a \to 0$, the composite system can be reduced to an isolated passive cavity. We find that, in the passive-passive double-cavity system, a strong photon-tunneling effect

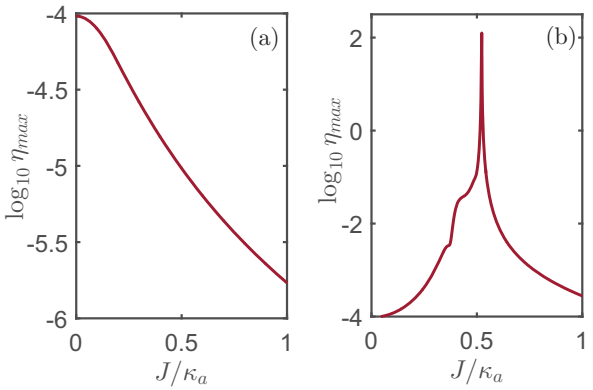

FIG. 3. The logarithm of the maximum value of η varies with the coupling strength J for (a) the passive-passive double-cavity system and (b) the passive-active double-cavity $\mathcal{PT}$ system. The other system parameters are the same as in Fig. 2.

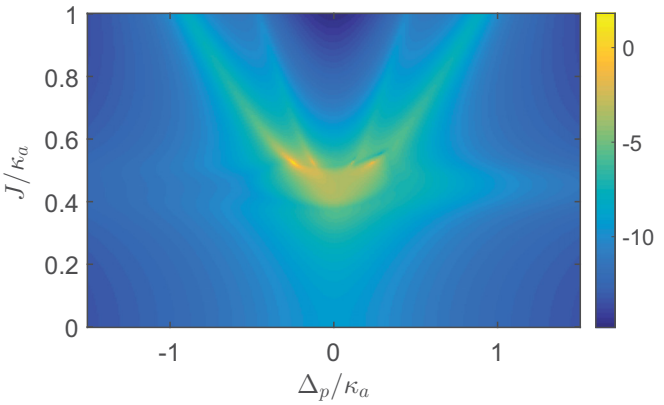

FIG. 4. The logarithm of η versus the detuning Δ_p/κ_a and the coupling strength J/κ_a for the $\mathcal{PT}$-symmetric system. The other system parameters are the same as in Fig. 2.

is adverse to the second-order sideband generation: $\eta_{\max}$ decreases exponentially with the increase of J. However, the obtained results for the $\mathcal{PT}$-symmetric double-cavity system are quite different from the passive-passive double-cavity system. It is obvious from Fig. 3(b) that, with the increase of J, $\eta_{\max}$ goes through exponential growth in the $\mathcal{PT}$-broken phase and exponential reduction in the $\mathcal{PT}$-symmetric phase, reaching its maximum value in the vicinity of $J/\kappa_a = 0.5$. Apparently the $\mathcal{PT}$-symmetric structure can enhance the second-order sideband significantly, especially in the vicinity of EP.

Physically the Kerr nonlinearity strength of the system plays an important role in generating the second-order or higher-order sideband processes. Generally speaking, in an optical cavity with an embedded nonlinear medium, a biharmonic control and probe laser launched into a cavity mode can excite multiwave-mixing processes via an optical nonlinearity effect [1], which thus produce a series of optical high-order sidebands. On the other hand, as shown in Ref. [53], in the vicinity of EP, the field localization can induce the dynamical accumulations of optical energy in the two supermode-based cavities, corresponding to an increasing intracavity nonlinearity. Hence the enhanced high-order sidebands can be generated by this $\mathcal{PT}$-induced strong nonlinearity. It should be pointed out that, owing to the existence of an additional nonlinear term [see Eq. (2)] in the $\mathcal{PT}$-symmetric system, the maximum value of η is not achieved exactly at the EP but shifts a small value [53].

Finally, in order to illustrate the impact of the photon-tunneling effect on the second-order sideband generation in the $\mathcal{PT}$-symmetric system more detail, we plot the logarithm of η versus the detuning Δ_p and the coupling strength J in Fig. 4. In the $\mathcal{PT}$-broken phase, η shows a marked increase at $\Delta_p = 0$ with the increase of J. The emergence of the yellow zone confirms that the robust second-order sideband can be achieved around the EP. As the system enters into the $\mathcal{PT}$-symmetric phase, four cyan bright lines split from the yellow zone, representing four peak values of η. Moreover the positions of sideband peaks are far away from $\Delta_p = 0$ with the increasing J, and the peak values are gradually decreased as shown in Fig. 4.

B. Dependence of the second-order sideband on the Kerr nonlinearity U

It is well known that the EP marks the $\mathcal{PT}$-symmetric phase and $\mathcal{PT}$-broken phase. The EP is obtained by diagonalizing the coefficient matrix of Eqs. (2) and (3) without considering the nonlinear term induced by the Kerr nonlinearity. However, when the nonlinear term is taken into account, the phase transition point of the $\mathcal{PT}$- symmetric system is upper shifted slightly [32,57], under which the $\mathcal{PT}$-broken phase is enlarged and the $\mathcal{PT}$-symmetric phase is narrowed. In view of this, the parameters we chosen in Fig. 5 and all the other figures in the paper are far from the phase transition point to ensure the correctness of the results. In addition, we have shown in the above discussion that the spectrums of the second-order sideband in the $\mathcal{PT}$-broken phase and $\mathcal{PT}$-symmetric phase are different, and its value increases in the $\mathcal{PT}$-broken phase and decreases in the $\mathcal{PT}$-symmetric phase with the increasing coupling strength J. Those characteristics of the second-order sideband may offer a new method to distinguish the $\mathcal{PT}$-symmetric phase and $\mathcal{PT}$-broken phase.

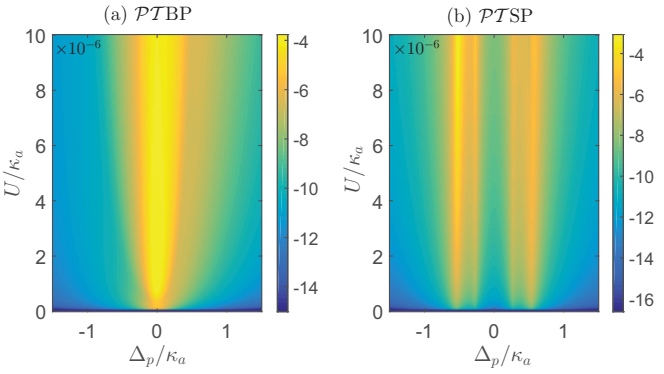

FIG. 5. The logarithm of η versus the detuning Δ_p/κ_a and the nonlinearity strength U/κ_a for the $\mathcal{PT}$-symmetric system. We use the coupling strength $J/\kappa_a = 0.4$ in panel (a) and $J/\kappa_a = 0.7$ in panel (b), corresponding respectively to the $\mathcal{PT}$-broken phase ($\mathcal{PT}$BP) and $\mathcal{PT}$-symmetric phase ($\mathcal{PT}$SP). The other system parameters are the same as in Fig. 2.

For the present $\mathcal{PT}$-symmetric system, the logarithm of η varying with Δ_p and U is plotted in Fig. 5(a) corresponding to the $\mathcal{PT}$-broken phase ($\mathcal{PT}$BP) and Fig. 5(b) corresponding to the $\mathcal{PT}$-symmetric phase ($\mathcal{PT}$SP). As we can see from Fig. 5 the increased nonlinearity can arouse considerable enhancement of η in both $\mathcal{PT}$BP and $\mathcal{PT}$SP. We note that the yellow zone in Fig. 5(a) is brighter than that in Fig. 5(b). This is due to the effect of field localization in the $\mathcal{PT}$BP, where the intracavity intensity can be accumulated, giving rise to strong effective nonlinearity [17,53]. Therefore, in this condition, the efficiency of the second-order sideband generation in the $\mathcal{PT}$BP is more improved. We also note that, in the $\mathcal{PT}$SP, the two yellow lines on the left are gradually brighter than the right two with the increase of U. The nonlinearity-induced enhancement of the second-order sideband seems mainly concentrated on the left side of $\Delta_p = 0$. The basic reason for these phenomena is that the phase transition point shifts with the increase of the Kerr nonlinearity strength U and gradually approaches $J = 0.7\kappa_a$. This aggravates the asymmetric structure of the second-order sideband, as can be seen in Fig. 2(b).

C. Dependence of the second-order sideband on the cavity detuning Δ

The cavity detuning Δ ($\Delta = \omega - \omega_c$) also has a significant influence on the second-order sideband generation. In the following, we present the variation of η when the control field is modulated to be off-resonance with the cavity field ($\Delta \neq 0$) under three different regimes as shown in Figs. 6–8.

First, in the non-$\mathcal{PT}$-symmetric regime (see Fig. 6), we find that the symmetric structure of η in Fig. 6(a) is broken when $\Delta \neq 0$. One of the left peaks higher than the right one is displayed in Fig. 6(b) where three sideband peaks are observed. As Δ becomes large, we find four sideband peaks in Fig. 6(c),

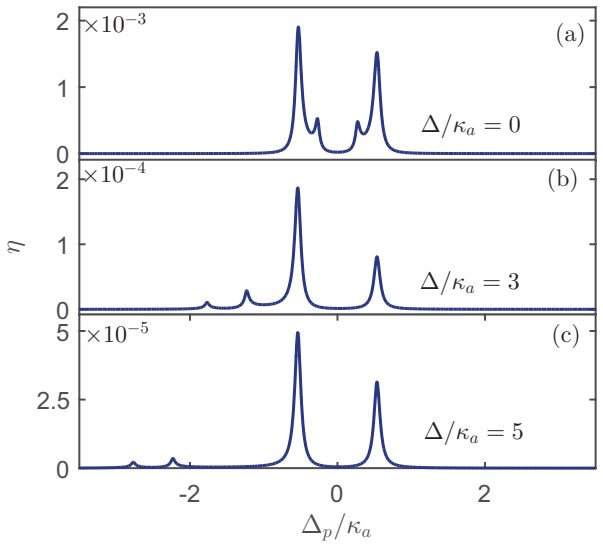

FIG. 7. Calculation result of η in the unbroken-$\mathcal{PT}$-symmetric regime versus the detuning Δ_p/κ_a under the same coupling strength $J/\kappa_a = 0.7$ for three different values of the cavity detuning Δ. We use $\Delta = 0$ in panel (a), $\Delta/\kappa_a = 3$ in panel (b), and $\Delta/\kappa_a = 5$ in panel (c). The other system parameters are the same as in Fig. 2.

indicating that the sideband peaks split again. However, the number of the sideband peaks is only up to four even though we further increase the detuning Δ. Meanwhile, the off-resonant laser weakens the intracavity field, resulting in the reduction of η. Second, we concentrate on the case that the control field is off-resonance with the cavity field in the unbroken-$\mathcal{PT}$-symmetric regime (see Fig. 7). With the increase of Δ, two of the sideband peaks shift towards the direction of $\Delta_p < 0$, far away from the resonance condition, while the other two remain unchanged still. The stronger Δ is, the more the peaks shift. At

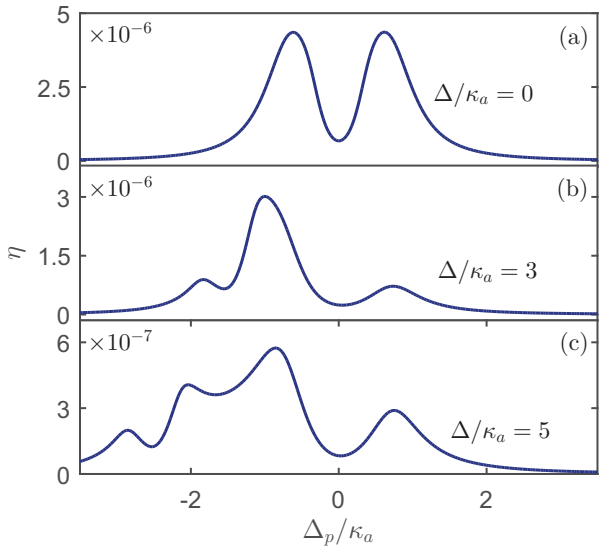

FIG. 6. Calculation result of η in the non-$\mathcal{PT}$-symmetric regime versus the detuning Δ_p/κ_a under the same coupling strength $J/\kappa_a = 0.7$ for three different values of the cavity detuning Δ. We use $\Delta = 0$ in panel (a), $\Delta/\kappa_a = 3$ in panel (b), and $\Delta/\kappa_a = 5$ in panel (c). The other system parameters are the same as in Fig. 2.

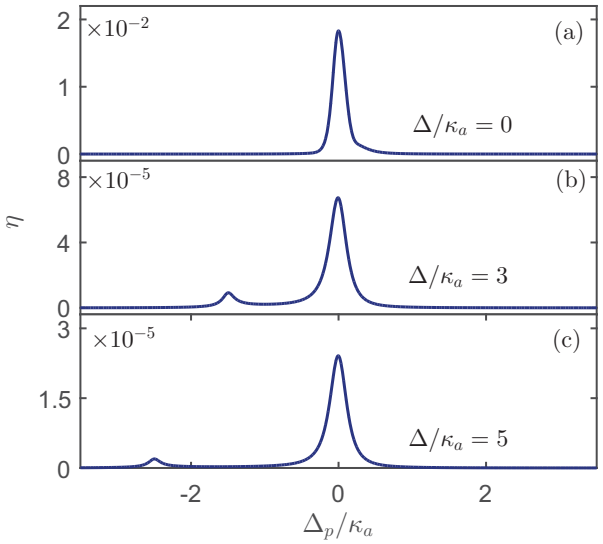

FIG. 8. Calculation result of η in the broken-$\mathcal{PT}$-symmetric regime versus the detuning Δ_p/κ_a under the same coupling strength $J/\kappa_a = 0.4$ for three different values of the cavity detuning Δ. We use $\Delta = 0$ in panel (a), $\Delta/\kappa_a = 3$ in panel (b), and $\Delta/\kappa_a = 5$ in panel (c). The other system parameters are the same as in Fig. 2.

the same time, the second-order sideband generation becomes less efficient. The phenomenon of the sideband peak shift can also be observed when $\Delta < 0$. The only difference is that they move in the opposite direction (i.e., the direction of $\Delta_p > 0$). Alternatively, we adjust the coupling strength to $J/\kappa_a = 0.4$, which puts the system in the broken-$\mathcal{PT}$-symmetric regime. From Fig. 8, we find that the single sideband peak splits into two asymmetric peaks: one stationary peak at $\Delta_p = 0$ and one mobile peak traveling with the change of Δ.

In view of these discussions above, we can summarize the following features under the influence of Δ on η: (i) the reduction of the second-order sideband generation is obvious when the control laser is off-resonance with the cavity field, and η decreases as the detuning Δ increases; (ii) the cavity detuning brings out multipeak structure of η in the non-$\mathcal{PT}$-symmetric regime and broken-$\mathcal{PT}$-symmetric regime, which complicates the spectrum of the second-order sideband; and (iii) the amount of the detuning-induced peak has a ceiling, and furthermore those peaks are shifted according to the variation of Δ.

D. Generation of optical higher-order sidebands in $\mathcal{PT}$-symmetric arrangements

In all of the above discussions, we focus on the second-order sideband in the output field based on the analytical solution (20) by the perturbation method. Now we turn to discuss the higher-order sideband generation by the numerical simulations according to Eqs. (2) and (3). Figure 9 shows the higher-order sideband spectra generated for the two different configurations: (i) the passive-passive double-cavity system [see Fig. 9(a)] and (ii) the $\mathcal{PT}$-symmetric (i.e., passive-active) double-cavity system [see Fig. 9(b)]. As can be seen in Fig. 9, the introduction of the $\mathcal{PT}$-symmetric ideas affects significantly the magnitude of the respective high-order sidebands in the output spectra. Specifically, for the case of the passive-passive double cavity ($\kappa_b/\kappa_a = 0.8$) in Fig. 9(a), the positive and negative second-order sidebands ($n = \pm 2$), the third-order sidebands ($n = \pm 3$), and the higher-order sidebands are created. The observed sidebands are spaced at multiples of the beating frequency Ω between the two-tone driving components around the rotating frequency ω_c. As a result, the frequency of the high-order sideband of order n can be formulated by the relationship $\omega_n = \omega_c \pm n\Omega$, where n is the number of the sideband, $n = 0$ corresponds to the control field ω_c, and $n = 1$ corresponds to the probe field $\omega_p = \omega_c + \Omega$. It is obvious that the amplitude of the sidebands decreases quickly as the order of the sidebands increases gradually. For the case of the $\mathcal{PT}$-symmetric double cavity ($\kappa_b/\kappa_a = -0.8$) in Fig. 9(b), the amplitude of the high-order sidebands is largely enhanced with respect to Fig. 9(a) due to the $\mathcal{PT}$-induced strong nonlinearity [53]. Furthermore, the number of the high-order sidebands increases obviously. From what has been analyzed above, we can reach the conclusion that the significantly enhanced high-order sidebands can be achieved by introducing the $\mathcal{PT}$ symmetry, compared with the configuration of the passive-passive double cavity.

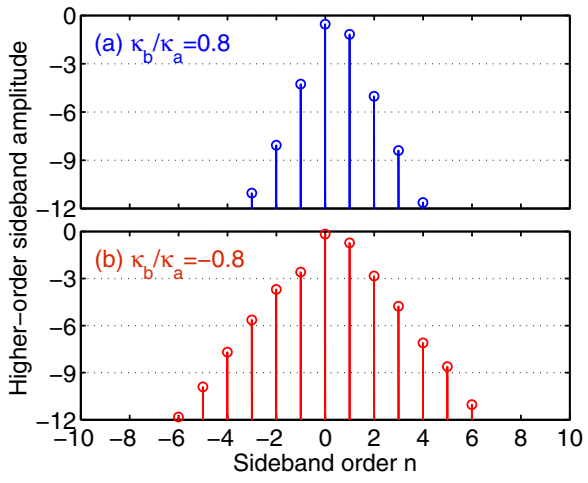

FIG. 9. Transmitted output (in logarithmic scale) of the generated higher-order sidebands for (a) the passive-passive double-cavity system (i.e., $\kappa_b/\kappa_a = 0.8$) and (b) the passive-active double-cavity $\mathcal{PT}$ system (i.e., $\kappa_b/\kappa_a = -0.8$) when $\Omega/\kappa_a = 0.25$ and $\Delta_p = \Omega$. Care was taken in normalizing the amplitude of the high-order sidebands to the input laser amplitude. The other system parameters used for the simulations are the same as in Figs. 2(b) and 2(d).

IV. EXPERIMENTAL REALIZATION OF OUR PROPOSED SCHEME

In this section we give a concise description that our proposal can be realized with the existing experimental techniques of microcavities with Kerr-type nanostructured materials. Optical macrocavities, such as Fabry-Perot macrocavities, whispering gallery macrocavities, and photonic crystals macrocavities, are widely used in variety of devices on account of its relatively high-quality factor Q and small mode volume V, which have the potential to enhance the light-matter interactions or cavity-atom coupling [58]. They usually have Q factors between 10^4 and 10^8 (a quality factor Q of 10^9 has been realized in silica microspheres resonators). The quality factor can be simplified as $Q = \omega/\kappa$ (κ is the cavity field decay rate). For the telecom wavelength of 1550 nm, the decay rates of microcavities range from 10^6 to 10^{10}.

Two directly coupled whispering gallery modes of silica can be used to implement our proposal. The whispering gallery modes can be found in cavities with geometries of spheres, disks, rings, and others. In Refs. [36,38,59,60], two whispering gallery microtoroidal resonators manufactured at the edges of two separate silicon chips are used to construct a $\mathcal{PT}$-symmetric dimer. The coupling strength between the resonators can be tuned by controlling the distance between the chips. One of the resonators doped with rare-earth ions (Er^{3+}), is pumped by a laser in 1460 nm wavelength band, which can provide optical gain to the resonator with an effective gain in 1550 nm band. In addition, the two resonators are coupled only in the latter wavelength band. The other one without dopant has passive loss.

In addition, a Kerr-type nonlinear material will be embedded in the passive resonator. The simplified photon-photon interaction can be approximated as $U_{nl} = \frac{3(\hbar\omega)^2\overline{\chi}^{(3)}}{4\epsilon_0 V_{\rm eff}\overline{\epsilon_r}^2}$. $V_{\rm eff}$ is the effective mode volume. $\overline{\chi}^{(3)}$ and $\overline{\epsilon_r}$ are the average real part of the nonlinear susceptibility and relative dielectric permittivity,

respectively [61,62]. The order of magnitude for the real part of the third-order susceptibility of the materials (such as Si or GaAs) is in the range of 10^{-19}–10^{-18} in Si units (m^2/V^2) [1]. For a near infrared wavelength (i.e. $\lambda = 1550$ nm), and the diffraction limited confinement volumes [$V_{\text{eff}} = (\lambda/2n_r)^3$], U_{nl} is estimated on the order of 10^{-3} μeV. The largest Kerr nonlinearity interaction strength in the proposal for the passive resonator is about $U = 3$ KHz, which can be achieved easily by the Si and GaAs material. We believe that other types of optical microcavities also can be used to implement the proposal, even if no corresponding experiments have been reported.

V. DISCUSSION AND SUMMARY

Before ending this paper, we give a few brief discussions on the notion of broken and unbroken $\mathcal{PT}$ symmetries in the present nonlinear dimer of two coupled single-mode cavities with gain and loss. First, we would like to point out that the passive-active double-cavity system we consider here possesses a phase transition from $\mathcal{PT}$-broken phase to the $\mathcal{PT}$-symmetric phase. This critical phase transition point is often referred to the spontaneous $\mathcal{PT}$ symmetry breaking point and also called the EP. The EP is obtained by diagonalizing the coefficient matrix of Eqs. (2)–(3) under the condition of ignoring the small EP shift induced by the nonlinear term $2iU|a|^2a$. Generally speaking, $\mathcal{PT}$-symmetric systems are investigated under the balanced gain and loss. However, it is difficult to implement the balanced gain-to-loss ratio exactly in the experiment. Various uncontrolled loss mechanisms, pump inhomogeneities, and other reasons [38,56] may be obstacles of the operation on the ideal balanced condition. In order to guarantee the feasibility of the experiment, we operate our work under the case that the gain-to-loss ratio is equal to -0.8 (or 0.8), which is very close to the ideal balanced condition. Moreover, the situation of unbalanced gain and loss in the cavity dimer is an extension of the balanced condition, also called $\mathcal{PT}$ symmetry [51,56]. In fact, a few works about $\mathcal{PT}$-symmetric lasers have broadened the definition of $\mathcal{PT}$-symmetric concepts to those without physically balanced gain and loss, such as the ones considered in Refs. [13,43–45,63]. For the unbalanced gain and loss ($\kappa_a \neq -\kappa_b$), the EP can be defined by $J = (\kappa_a - \kappa_b)/4$ when $\omega_a = \omega_b$ [43]. Second, the so-called broken and unbroken $\mathcal{PT}$ symmetries in all of the above discussions hold only in the linear limit [without considering Kerr nonlinearity in Eq. (1)]. That is to say, the dimer system is appropriately tuned so that it would be $\mathcal{PT}$-symmetric phase or $\mathcal{PT}$-broken phase in the linear regime (assuming $U = 0$). This method has described quantitatively the results of several experimental papers [36,38,44] and has been used in several theoretical literatures [17,32,51,53]. Strictly speaking, in the nonlinear regime here (with considering essential Kerr nonlinearity), the introduced nonlinearity will affect the $\mathcal{PT}$-symmetric structure of the dimer system including distinct $\mathcal{PT}$-symmetric or $\mathcal{PT}$-broken phases. However, the actual correspondence is not shown further for our proposed nonlinear model due to some tediously long calculations. It should be emphasized that, in our case, since we consider the dimer system in which a gain cavity is coupled to a lossy cavity with very weak Kerr nonlinearity, and hence this nonlinearity slightly shifts the transition point of the $\mathcal{PT}$-symmetric system as can be easily verified in Fig. 3(b). In this regard, for convenience we neglect the shift of the $\mathcal{PT}$-transition point induced by this weak nonlinearity. Addressing the correspondence of the two distinguished phases between the linear and nonlinear regimes is beyond the scope of the present work, and it will be taken into account more rigorously in future investigation by means of the numerical simulations.

In summary, we have theoretically explored the second-order and higher-order sideband generation and their robust control in a $\mathcal{PT}$-symmetric nonlinear structure composed of two directly coupled microcavities, with realistic system parameters. The analytical expression describing and featuring the second-order sideband is obtained by means of the perturbation method. We analyze the influences of the photon-tunneling rate, Kerr nonlinearity strength, and optical detuning on the second-order sideband generation. We find that the second-order sideband signal can be amplified considerably in the $\mathcal{PT}$-symmetric system. Since the effective optical nonlinearity can be greatly enhanced with the help of field-localization effect in the $\mathcal{PT}$-broken phase, the second-order sideband is improved sharply in vicinity of the phase transition point. We also illustrate the optical higher-order sideband generation by means of numerical simulations, where the higher-order sideband amplitude indeed is largely raised in this $\mathcal{PT}$-symmetric arrangement. Finally, an experimental feasibility of the proposed double cavity scheme is presented. Our study provides a new method of strong second- and high-order sideband generation with $\mathcal{PT}$-symmetric phase transition and relaxes the requirement of strong laser input, which is very meaningful for chip-scale optical communications and optical frequency combs.

Note added. Recently, we became aware of a related work on the arXiv preprint by Jiao *et al.* [64], in which a vibrational mechanical mode is used to induce optical nonlinearity for producing the delaying or advancing second-order sideband signal in active cavity optomechanics.

ACKNOWLEDGMENTS

We would like to express our sincerely appreciation to the referee for his or her careful reading of our manuscript and valuable suggestions, which significantly improved the paper. We thank Xiao-Xue Yang for useful advice and discussion in the manuscript preparation. We also are grateful to Rong Yu for sharing her codes from the numerical method of fast Fourier transformation. This research is supported in part by the National Natural Science Foundation of China (NSFC) under Grants No. 11375067 and No. 11574104, as well as the National Basic Research Program of China (973 Program) under Contract No. 2012CB922103.

[1] R. W. Boyd, *Nonlinear Optics* (Academic Press, New York, 2008).

[2] P. Franken, A. Hill, C. W. Peters, and G. Weinreich, Generation of Optical Harmonics, Phys. Rev. Lett. **7**, 118 (1961).

[3] H. Xiong, L.-G. Si, A.-S. Zheng, X. Yang, and Y. Wu, Higher-order sidebands in optomechanically induced transparency, Phys. Rev. A **86**, 013815 (2012).

[4] J. Li, R. Yu, and Y. Wu, Tunable higher-order sideband spectra in a waveguide-coupled photonic crystal molecule beyond the weak-excitation approximation, Phys. Rev. A **89**, 015802 (2014).

[5] J. Ma, C. You, L.-G. Si, H. Xiong, J. Li, and Y. Wu, Optomechanically induced transparency in the presence of an external time-harmonic-driving force, Sci. Rep. **5**, 11278 (2015).

[6] H. Suzuki, E. Brown, and R. Sterling, Nonlinear dynamics of an optomechanical system with a coherent mechanical pump: Second-order sideband generation, Phys. Rev. A **92**, 033823 (2015).

[7] C. M. Bender and S. Boettcher, Real Spectra in Non-Hermitian Hamiltonians Having $\mathcal{PT}$ Symmetry, Phys. Rev. Lett. **80**, 5243 (1998).

[8] A. Mostafazadeh, Pseudo-Hermiticity versus PT symmetry: The necessary condition for the reality of the spectrum of a non-Hermitian Hamiltonian, J. Math. Phys. **43**, 205 (2002).

[9] C. M. Bender, Introduction to $\mathcal{PT}$-symmetric quantum theory, Contemp. Phys. **46**, 277 (2005).

[10] R. El-Ganainy, K. G. Makris, D. N. Christodoulides, and Z. H. Musslimani, Theory of coupled optical $\mathcal{PT}$-symmetric structures, Opt. Lett. **32**, 2632 (2007).

[11] K. G. Makris, R. El-Ganainy, D. N. Christodoulides, and Z. H. Musslimani, Beam Dynamics in $\mathcal{PT}$-Symmetric Optical Lattices, Phys. Rev. Lett. **100**, 103904 (2008).

[12] Z. H. Musslimani, K. G. Makris, R. El-Ganainy, and D. N. Christodoulides, Optical Solitons in $\mathcal{PT}$ Periodic Potentials, Phys. Rev. Lett. **100**, 030402 (2008).

[13] L. Ge, Y. Chong, S. Rotter, H. Türeci, and A. Stone, Unconventional modes in lasers with spatially varying gain and loss, Phys. Rev. A **84**, 023820 (2011).

[14] C. M. Bender, M. Gianfreda, S. K. Özdemir, B. Peng, and L. Yang, Twofold transition in $\mathcal{PT}$-symmetric coupled oscillators, Phys. Rev. A **88**, 062111 (2013).

[15] M. Zhang, G. S. Wiederhecker, S. Manipatruni, A. Barnard, P. McEuen, and M. Lipson, Synchronization of Micromechanical Oscillators Using Light, Phys. Rev. Lett. **109**, 233906 (2012).

[16] N. Bender, S. Factor, J. D. Bodyfelt, H. Ramezani, D. N. Christodoulides, F. M. Ellis, and T. Kottos, Observation of Asymmetric Transport in Structures with Active Nonlinearities, Phys. Rev. Lett. **110**, 234101 (2013).

[17] Z.-P. Liu, J. Zhang, S. K. Özdemir, B. Peng, H. Jing, X.-Y. Lü, C.-W. Li, L. Yang, F. Nori, and Y.-X. Liu, Metrology with $\mathcal{PT}$-symmetric cavities: Enhanced sensitivity near the $\mathcal{PT}$-phase transition, arXiv:1510.05249v1.

[18] L. Ge, Parity-time symmetry in a flat-band system, Phys. Rev. A **92**, 052103 (2015).

[19] J. Wiersig, Sensors operating at exceptional points: General theory, Phys. Rev. A **93**, 033809 (2016).

[20] K. V. Kepesidis, T. J. Milburn, K. G. Makris, S. Rotter, and P. Rabl, $\mathcal{PT}$-symmetry breaking in the steady state, arXiv:1508.00594v1.

[21] R. El-Ganainy, K. G. Makris, and D. N. Christodoulides, Local $\mathcal{PT}$ invariance and supersymmetric parametric oscillators, Phys. Rev. A **86**, 033813 (2012).

[22] G. S. Agarwal and K. Qu, Spontaneous generation of photons in transmission of quantum fields in PT-symmetric optical systems, Phys. Rev. A **85**, 031802 (2012).

[23] T. Oishi and M. Tomita, Inverted coupled-resonator-induced transparency, Phys. Rev. A **88**, 013813 (2013).

[24] H. Jing, S. K. Özdemir, X.-Y. Lü, J. Zhang, L. Yang, and F. Nori, $\mathcal{PT}$-Symmetric Phonon Laser, Phys. Rev. Lett. **113**, 053604 (2014).

[25] H. Hodaei, M.-A. Miri, M. Heinrich, D. N. Christodoulides, and M. Khajavikhan, Parity-time-symmetric microring lasers, Science **346**, 975 (2014).

[26] X.-W. Xu, Y.-x. Liu, C.-P. Sun, and Y. Li, Mechanical $\mathcal{PT}$ symmetry in coupled optomechanical systems, Phys. Rev. A **92**, 013852 (2015).

[27] D. D. Scott and Y. N. Joglekar, Degrees and signatures of broken $\mathcal{PT}$ symmetry in nonuniform lattices, Phys. Rev. A **83**, 050102 (2011).

[28] E.-M. Graefe and H. F. Jones, $\mathcal{PT}$-symmetric sinusoidal optical lattices at the symmetry-breaking threshold, Phys. Rev. A **84**, 013818 (2011).

[29] A. E. Miroshnichenko, B. A. Malomed, and Y. S. Kivshar, Nonlinearly $\mathcal{PT}$-symmetric systems: Spontaneous symmetry breaking and transmission resonances, Phys. Rev. A **84**, 012123 (2011).

[30] I. V. Barashenkov, L. Baker, and N. V. Alexeeva, $\mathcal{PT}$-symmetry breaking in a necklace of coupled optical waveguides, Phys. Rev. A **87**, 033819 (2013).

[31] X. Luo, J. Huang, H. Zhong, X. Qin, Q. Xie, Y. S. Kivshar, and C. Lee, Pseudo-Parity-Time Symmetry in Optical Systems, Phys. Rev. Lett. **110**, 243902 (2013).

[32] H. Ramezani, T. Kottos, R. El-Ganainy, and D. N. Christodoulides, Unidirectional nonlinear $\mathcal{PT}$-symmetric optical structures, Phys. Rev. A **82**, 043803 (2010).

[33] L. Feng, M. Ayache, J. Huang, Y.-L. Xu, M.-H. Lu, Y.-F. Chen, Y. Fainman, and A. Scherer, Nonreciprocal light propagation in a silicon photonic circuit, Science **333**, 729 (2011).

[34] Z. Lin, H. Ramezani, T. Eichelkraut, T. Kottos, H. Cao, and D. N. Christodoulides, Unidirectional Invisibility Induced by $\mathcal{PT}$-Symmetric Periodic Structures, Phys. Rev. Lett. **106**, 213901 (2011).

[35] L. Feng, Y.-L. Xu, W. S. Fegadolli, M.-H. Lu, J. E. Oliveira, V. R. Almeida, Y.-F. Chen, and A. Scherer, Experimental demonstration of a unidirectional reflectionless parity-time metamaterial at optical frequencies, Nat. Mater. **12**, 108 (2013).

[36] L. Chang, X. Jiang, S. Hua, C. Yang, J. Wen, L. Jiang, G. Li, G. Wang, and M. Xiao, Parity-time symmetry and variable optical isolation in active-passive-coupled microresonators, Nat. Photon. **8**, 524 (2014).

[37] X. Liu, S. D. Gupta, and G. S. Agarwal, Regularization of the spectral singularity in $\mathcal{PT}$-symmetric systems by all-order nonlinearities: Nonreciprocity and optical isolation, Phys. Rev. A **89**, 013824 (2014).

[38] B. Peng, S. K. Özdemir, F. Lei, F. Monifi, M. Gianfreda, G. L. Long, S. Fan, F. Nori, C. M. Bender, and L. Yang, Parity-time-symmetric whispering-gallery microcavities, Nat. Phys. **10**, 394 (2014).

[39] J. Wiersig, Enhancing the Sensitivity of Frequency and Energy Splitting Detection by Using Exceptional Points: Application to Microcavity Sensors for Single-Particle Detection, Phys. Rev. Lett. **112**, 203901 (2014).

[40] R. Fleury, D. Sounas, and A. Alú, An invisible acoustic sensor based on parity-time symmetry, Nat. Commun. **6**, 5905 (2015).
[41] B. Peng, S. K. Özdemir, S. Rotter, H. Yilmaz, M. Liertzer, F. Monifi, C. M. Bender, F. Nori, and L. Yang, Loss-induced suppression and revival of lasing, Science **346**, 328 (2014).
[42] L. Feng, Z. J. Wong, R.-M. Ma, Y. Wang, and X. Zhang, Single-mode laser by parity-time symmetry breaking, Science **346**, 972 (2014).
[43] R. El-Ganainy, M. Khajavikhan, and L. Ge, Exceptional points and lasing self-termination in photonic molecules, Phys. Rev. A **90**, 013802 (2014).
[44] M. Brandstetter, M. Liertzer, C. Deutsch, P. Klang, J. Schöberl, H. Türeci, G. Strasser, K. Unterrainer, and S. Rotter, Reversing the pump dependence of a laser at an exceptional point, Nat. Commun. **5**, 4034 (2014).
[45] M. Liertzer, L. Ge, A. Cerjan, A. D. Stone, H. Türeci, and S. Rotter, Pump-Induced Exceptional Points in Lasers, Phys. Rev. Lett. **108**, 173901 (2012).
[46] S. Longhi and L. Feng, $\mathcal{PT}$-symmetric microring laser-absorber, Opt. Lett. **39**, 5026 (2014).
[47] Y. Chong, L. Ge, and A. D. Stone, $\mathcal{PT}$-Symmetry Breaking and Laser-Absorber Modes in Optical Scattering Systems, Phys. Rev. Lett. **106**, 093902 (2011).
[48] A. Guo, G. Salamo, D. Duchesne, R. Morandotti, M. Volatier-Ravat, V. Aimez, G. Siviloglou, and D. Christodoulides, Observation of $\mathcal{PT}$-Symmetry Breaking in Complex Optical Potentials, Phys. Rev. Lett. **103**, 093902 (2009).
[49] H. Jing, S. K. Özdemir, Z. Geng, J. Zhang, X.-Y. Lü, B. Peng, L. Yang, and F. Nori, Optomechanically-induced transparency in parity-time-symmetric microresonators, Sci. Rep. **5**, 9663 (2015).
[50] R. El-Ganainy, J. I. Dadap, and R. M. Osgood, Optical parametric amplification via non-Hermitian phase matching, Opt. Lett. **40**, 5086 (2015).
[51] X.-Y. Lü, H. Jing, J.-Y. Ma, and Y. Wu, $\mathcal{PT}$-Symmetry-Breaking Chaos in Optomechanics, Phys. Rev. Lett. **114**, 253601 (2015).
[52] B. He, S.-B. Yan, J. Wang, and M. Xiao, Quantum noise effects with Kerr-nonlinearity enhancement in coupled gain-loss waveguides, Phys. Rev. A **91**, 053832 (2015).
[53] J. Zhang, B. Peng, S. K. Özdemir, Y.-X. Liu, H. Jing, X.-Y. Lü, Y.-l. Liu, L. Yang, and F. Nori, Giant nonlinearity via breaking parity-time symmetry: A route to low-threshold phonon diodes, Phys. Rev. B **92**, 115407 (2015).
[54] J. Li, X. Zhan, C. Ding, D. Zhang, and Y. Wu, Enhanced nonlinear optics in coupled optical microcavities with an unbroken and broken parity-time symmetry, Phys. Rev. A **92**, 043830 (2015).
[55] S. Weis, R. Rivière, S. Deléglise, E. Gavartin, O. Arcizet, A. Schliesser, and T. J. Kippenberg, Optomechanically induced transparency, Science **330**, 1520 (2010).
[56] H. Hodaei, M.-A. Miri, A. U. Hassan, W. E. Hayenga, M. Heinrich, D. N. Christodoulides, and M. Khajavikhan, Single mode lasing in transversely multi-moded PT-symmetric microring resonators, Laser Photon. Rev. **10**, 494 (2016).
[57] H. Cartarius, D. Haag, D. Dast, and G. Wunner, Nonlinear Schrödinger equation for a $\mathcal{PT}$-symmetric delta-function double well, J. Phys. A: Math. Theor. **45**, 444008 (2012).
[58] K. J. Vahala, Optical microcavities, Nature (London) **424**, 839 (2003).
[59] H. Hodaei, M. A. Miri, A. U. Hassan, W. E. Hayenga, M. Heinrich, D. N. Christodoulides, and M. Khajavikhan, Parity-time-symmetric coupled microring lasers operating around an exceptional point, Opt. Lett. **40**, 4955 (2015).
[60] A. U. Hassan, H. Hodaei, M.-A. Miri, M. Khajavikhan, and D. N. Christodoulides, Nonlinear reversal of the $\mathcal{PT}$-symmetric phase transition in a system of coupled semiconductor microring resonators, Phys. Rev. A **92**, 063807 (2015).
[61] S. Ferretti and D. Gerace, Single-photon nonlinear optics with Kerr-type nanostructured materials, Phys. Rev. B **85**, 033303 (2012).
[62] T. K. Fryett, C. M. Dodson, and A. Majumdar, Cavity enhanced nonlinear optics for few photon optical bistability, Opt. Express **23**, 16246 (2015).
[63] L. Ge and R. El-Ganainy, Nonlinear modal interactions in parity-time ($\mathcal{PT}$) symmetric lasers, Sci. Rep. **6**, 24889 (2016).
[64] Y. Jiao, H. Lü, J. Qian, Y. Li, and H. Jing, Amplifying higher-order sidebands in optomechanical transparency with gain and loss, arXiv:1602.05308v2.